Non-Muffin-Tin Atomic Scattering-Matrices for Semiconductor LEED-Calculations

J.-V. Peetz and W. Schattke

Institut für Theoretische Physik, Universität Kiel,
Leibnizstr. 15, D-24118 Kiel, Germany.

Non-muffin-tin potentials for LEED-calculations can be treated by the integration of the Lippmann-Schwinger equation as described by Nagano and Tong. We have solved this coupled system of equations numerically with a code for ordinary differential equations. The general scattering potential is generated by superimposing atomic Clementi-Roetti densities and Coulomb potentials for a cluster of crystal atoms. The exchange potential is modeled as a function of the superimposed electron density. Both, energy-dependent and energy-independent exchange potentials are investigated. The spherical wave decomposition of the potential entering the angular momentum representation of the Lippmann-Schwinger equation is performed with an efficient numerical integration algorithm. Spherical wave components of the superposition potential are shown to emphasize their influence on the LEED-calculation. Scattering amplitudes of this potential model are computed and compared with those of standard muffin-tin phase shifts of GaAs. Especially, surface configurations are considered within this procedure.

1. INTRODUCTION

The development of a concept for the generalization of muffin-tin calculations to non-spherical systems, essentially its numerical realization, is an active field of research [1]. The application covers many cases which usually are treated by KKR bandstructure methods, e.g. in electron spectroscopy the photoemission and LEED calculations [2, 3]. This investigation is to be seen in the context of LEED and VLEED calculations performed for the surfaces of the III-V semiconductors where especially the open surfaces as that of GaAs$(\bar{1},\bar{1},\bar{1})2\times 2$ are rather peculiar because of the relative large reliability factors. One reason for these deviations should be attributed to the usual assumption of spherical muffin-tin potentials. Related difficulties are found in the one-step photoemission calculations of semiconductors where the muffin-tin approximation fails, too, which is sometimes circumvented by addition of empty spheres [2]. Because of the expensive numerical effort of such kind of calculations the solution of the latter problem has been postponed for a long time.

The subsequent analyzation originates from the concept of Nagano and Tong [4] and establishes a computer code for the calculation of scattering t-matrices of non-muffin-tin potentials. From this point of view it is the main step for the development of a full potential dynamical LEED program.

2. THEORY

2.1. Scattering theory

Following Nagano and Tong [4] we calculate the scattering of an electron by the general potential of a crystal-atom

$$V(\mathbf{r}) = \sum_L V_L(r) Y_L(\hat{\mathbf{r}})\,, \tag{1}$$

where $L = (l, m)$, and $Y_L(\hat{\mathbf{r}})$ is a spherical harmonic, via the Lippmann-Schwinger equation

$$\psi_{\mathbf{k}}(\mathbf{r}) = \varphi_{\mathbf{k}}(\mathbf{r}) + \int d\mathbf{r}_1\, G_0(k, \mathbf{r}-\mathbf{r}_1) V(\mathbf{r}_1)\psi_{\mathbf{k}}(\mathbf{r}_1)\,. \tag{2}$$

Here $\varphi_{\mathbf{k}}(\mathbf{r})$ is an incident plane wave with wave vector $\mathbf{k}$, $G_0(k, \mathbf{r}-\mathbf{r}_1)$ a single-particle Green's function, $k = \sqrt{(m_e/\hbar^2)2E}$, and $\psi_{\mathbf{k}}(\mathbf{r})$ the total wave function. The scattering t-matrix or transition matrix is defined by

$$\int d\mathbf{r}_2\, t(\mathbf{r}_1, \mathbf{r}_2)\varphi_{\mathbf{k}}(\mathbf{r}_2) = V(\mathbf{r}_1)\psi_{\mathbf{k}}(\mathbf{r}_1)\,. \tag{3}$$

In the angular-momentum representation we write

$$\varphi_{\mathbf{k}}(\mathbf{r}) = \sum_L 4\pi i^l j_l(kr) Y_L(\hat{\mathbf{r}}) Y_L^*(\hat{\mathbf{k}})\,,$$

$$G_0(k, \mathbf{r}-\mathbf{r}') = -\frac{m_e}{\hbar^2}\, 2ik \times \sum_L j_l(kr_<) h_l^{(1)}(kr_>) Y_L(\hat{\mathbf{r}}) Y_L^*(\hat{\mathbf{r}}')\,,$$

and

$$\psi_{\mathbf{k}}(\mathbf{r}) = \sum_{L,L'} 4\pi i^{l'} F_{k,LL'}(r) Y_L(\hat{\mathbf{r}}) Y_{L'}^*(\hat{\mathbf{k}})\,,$$

where $j_l(kr)$ and $h_l^{(1)}(kr)$ are spherical Bessel and Hankel functions of the first kind, and $r_< = \min(r,r')$, $r_> = \max(r,r')$. Recasting the Lippmann-Schwinger equation (2) into this representation Nagano and Tong [4] derive the following integral equation system of Volterra type

$$f_{k,LL'}(r) = j_l(kr) E_{k,LL'}(r) + i h_l^{(1)}(kr) S_{k,LL'}(r), \quad (4)$$

where we introduced

$$f_{k,LL'}(r) = \sum_{L_1} F_{k,LL_1}(r) E_{k,L_1L'}(\infty)\,,$$

$$E_{k,LL'}(r) = \delta_{LL'} + i\int_0^r dr'\, h_l^{(1)}(kr') \times \sum_{L_3} U_{k,LL_3}(r') f_{k,L_3L'}(r')\,,$$

$$S_{k,LL'}(r) = -\int_0^r dr'\, j_l(kr') \times \sum_{L_3} U_{k,LL_3}(r') f_{k,L_3L'}(r')\,,$$

$$U_{k,LL_3}(r) = \frac{m_e}{\hbar^2}\, 2k \sum_{L_2} C^L_{L_2L_3} r^2 V_{L_2}(r)\,,$$

and the Clebsch-Gordan-like coefficients

$$C^L_{L_2L_3} = \int d\Omega_{\mathbf{r}}\, Y_L^*(\hat{\mathbf{r}}) Y_{L_2}(\hat{\mathbf{r}}) Y_{L_3}(\hat{\mathbf{r}})\,.$$

The t-matrix as a function of wave vector modulus k in the angular-momentum representation reads

$$t_{LL'}(k) = i^{-(l-l')} \int d\mathbf{r}_1 \int d\mathbf{r}_2 \times j_l(kr_1) Y_L^*(\hat{\mathbf{r}}_1)\, t(\mathbf{r}_1,\mathbf{r}_2)\, j_{l'}(kr_2) Y_{L'}(\hat{\mathbf{r}}_2)$$

and Nagano and Tong [4] show that equation (3) leads to

$$t_{LL'}(k) = -\frac{\hbar^2}{m_e}\frac{1}{2k}\, i^{-(l-l')} \times \sum_{L_1} S_{k,LL_1}(\infty) E^{-1}_{k,L_1L'}(\infty)\,. \quad (5)$$

For the numerical evaluation of the t-matrix we transform the Volterra integral equation system (4) into an ordinary differential equation system

$$E'_{k,LL'}(r) = i h_l^{(1)}(kr) \sum_{L_3} U_{k,LL_3}(r) \times \left[j_{l_3}(kr) E_{k,L_3L'}(r) + i h_{l_3}^{(1)}(kr) S_{k,L_3L'}(r) \right],$$

$$S'_{k,LL'}(r) = -j_l(kr) \sum_{L_3} U_{k,LL_3}(r) \times \left[j_{l_3}(kr) E_{k,L_3L'}(r) + i h_{l_3}^{(1)}(kr) S_{k,L_3L'}(r) \right],$$

with the initial values

$$E_{k,LL'}(0) = \delta_{LL'}\,,\ S_{k,LL'}(0) = 0\,.$$

For the numerical integration of the differential equation system we use the FORTRAN code of Shampine and Gordon [5].

2.2. The scattering potential

We construct the crystal potential starting with the atomic Coulomb potential $V_a(r)$

$$V_a(r) = \frac{e^2}{4\pi\epsilon_0}\left[-\frac{Z_a}{r} + \frac{4\pi}{r}\int_0^r dt\, t^2 \rho_a(t) + 4\pi \int_r^\infty dt\, t\rho_a(t) \right],$$

where $\rho_a(r)$ is the atomic electron density and Z_a the atomic number. ρ_a is calculated from Clementi-Roetti atomic wave functions [6]. The crystal electron density ρ_c is taken to be

$$\rho_c(\mathbf{r}) = \sum_a \rho_a(|\mathbf{r}-\mathbf{R}_a|)\,,$$

where $\mathbf{R}_a$ is the position of a crystal atom. In the summation we take into account all atoms in a certain neighborhood. Using Hara exchange [7] we model the crystal potential V_c as

$$V_c(\mathbf{r}) = \sum_a \left[V_a(|\mathbf{r}-\mathbf{R}_a|) + \frac{I}{r} \right] - \frac{e^2}{4\pi\epsilon_0}\left[\frac{2}{\pi} k_F(\mathbf{r}) F(\eta_E(\mathbf{r})) + \frac{MI^3}{d\,|I|} \right],$$

where I is the core ionicity, M the Madelung constant, and d the nearest neighbor distance. Furthermore we utilize

$$k_F(\mathbf{r}) = \left[3\pi^2 \rho_c(\mathbf{r})\right]^{1/3} ,$$

$$F(\eta) = \frac{1}{2} + \frac{1-\eta^2}{4\eta} \log\left|\frac{1+\eta}{1-\eta}\right|$$

$$\eta_E(\mathbf{r}) = k_i(\mathbf{r})/k_F(\mathbf{r}) ,$$

$$(k_i(\mathbf{r}))^2 = (k_F(\mathbf{r}))^2 + \frac{m_e}{\hbar^2} 2(E + |\varepsilon_{max}|) .$$

ε_{max} is the binding energy of the least bound occupied state of the ion-core and E the kinetic energy of the continuum electron, i.e. the LEED beam energy.

In order to apply multiple scattering theory we subdivide the crystal volume into Wigner-Seitz cells or more generally into Voronoi polyhedra, which contain at most one crystal atom. The single site potentials V_i are given by

$$V_i(\mathbf{r}) = V_c(\mathbf{r})\Theta_i(\mathbf{r}) ,$$

where the shape function $\Theta_i(\mathbf{r})$ restricts the potential to the ith polyhedron,

$$\Theta_i(\mathbf{r}) = \begin{cases} 1 & \text{if } \mathbf{r} \text{ is inside Voronoi} \\ & \text{polyhedron } i, \\ 0 & \text{otherwise.} \end{cases}$$

The coefficients $V_L(r)$ of equation (1) can be calculated as

$$V_L(r) = \int d\Omega_{\mathbf{r}}\, V(\mathbf{r}) Y_L^*(\hat{\mathbf{r}}) , \qquad (6)$$

where we consider a general Voronoi polyhedron and therefore have dropped the index i. Numerically we approximate the integral in equation (6) by a summation over weighted function values at discrete points. The points and weights are chosen for example of Gauss type as suggested by Lebedev [8]. Because of the discontinuities at the cell boundaries this procedure leads to discontinuities in the coefficients $V_L(r)$. To overcome this deficiency in a simple approach we soften the boundary step function $\Theta(\mathbf{r})$ following the ideas of Becke [9]. Within a distance a to the polyhedron plane defined by the neighbor atom at position $\mathbf{R}_j$ we replace the factor $\theta(R_j/2 - \mathbf{r}\cdot\mathbf{R}_j/R_j)$ in $\Theta(\mathbf{r})$ by the function

$$s(x) = \frac{1}{4}\left(2 - (3 - x^2)x\right) ,$$
$$\text{with } x = \frac{1}{a}\left(\mathbf{r}\cdot\mathbf{R}_j/R_j - R_j/2\right) .$$

In a future version we will instead use the angular-momentum decomposition of the shape-truncation function as proposed and calculated by Stefanou and Zeller [10].

2.3. The scattering amplitude

In the following we examine the scattering amplitude $A(\mathbf{k}', \mathbf{k})$ of our potential which is defined by

$$A(\mathbf{k}', \mathbf{k}) = -\frac{m_e}{\hbar^2}\frac{1}{2\pi} \times \int d\mathbf{r}\, \exp(-i\mathbf{k}'\cdot\mathbf{r}) V(\mathbf{r}) \psi_{\mathbf{k}}(\mathbf{r}) .$$

In terms of the transition matrix $t_{L'L}(k)$ (5) it becomes

$$A(\mathbf{k}', \mathbf{k}) = -\frac{m_e}{\hbar^2} 8\pi \sum_{L',L} Y_{L'}(\hat{\mathbf{k}}') t_{L'L}(k) Y_L^*(\hat{\mathbf{k}}).$$

Due to fundamental properties of the t-matrix the scattering amplitude obeys two important relations:

$$\frac{i}{2}\left[A^*(\mathbf{k}, \mathbf{k}') - A(\mathbf{k}', \mathbf{k})\right] = \frac{k}{4\pi} \int d\Omega_{\mathbf{k}_1}\, A^*(\mathbf{k}_1, \mathbf{k}') A(\mathbf{k}_1, \mathbf{k}) ,$$

which is known as the general optical theorem, and

$$A(\mathbf{k}', \mathbf{k}) = A(-\mathbf{k}, -\mathbf{k}')$$

which is called the reciprocity theorem. Our numerical results fulfilled these relations.

3. RESULTS

We calculated the potential and scattering amplitude for an arsenic atom in the GaAs(110) surface geometry. In the bulk geometry we took four next-nearest neighbor gallium and twelve next-nearest neighbor arsenic atoms into account, in the surface geometry we investigated an arsenic atom in the first layer without relaxation or reconstruction. At the surface we considered three

Ga and seven As neighbors for the arsenic atom. The Voronoi polyhedron was built with additional neighbor atoms, which did not contribute to the potential. For example the surface boundary was determined by a virtual neighbor atom in the vacuum. The cartesian coordinate system is assumed left-handed with the x-axis pointing perpendicular into the surface, the y- and z- axes being parallel to the surface. The mirror symmetry-plane of the GaAs(110) surface coincides with the xy-plane. The gallium neighbors, which are located in the same layer as the central As atom, have the coordinates (x, y, z) = (0, 1.414, ±2.000) Å. In the numerical evaluation of the t-matrix (5) we truncated the angular momentum series at $l_{\max} = 6$. For the potential we used all spherical wave components up to $l \leq 9$. Inclusion of higher angular momentum components altered the elements of the t-matrix only in the percentage range. For the parameter a, which softens the boundary step of the Voronoi polyhedron, a value of 0.1 Å was found to give appropriate smooth spherical wave components for the potential. In figure 1 we show the imaginary part of the $L = (3,1)$ spherical component for the bulk potential.

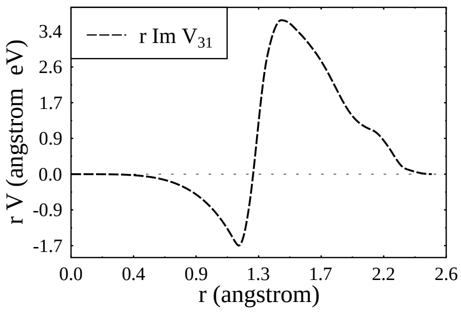

Fig. 1: $L = (3,1)$ spherical harmonic component of the potential of an As atom in the bulk of GaAs(110) for incident energy 50 eV and *fuzzy* parameter $a =$ 0.1 Å.

In figure 2 we plot some of the nonspherical parts of the potential for an arsenic atom in the GaAs(110) surface.

In both cases there are evident contributions to the scattering potential, especially between the muffin-tin radius $R_{MT} = 1.22$ Å and the radius of the Wigner-Seitz sphere $R_{WS} = 2.34$ Å.

In the following figures we analyze the angular

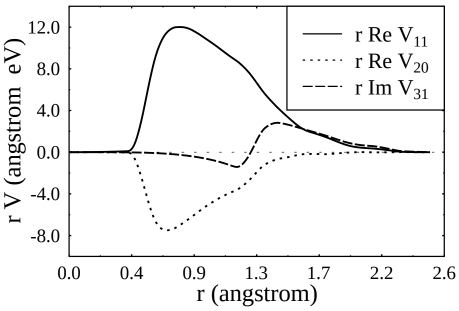

Fig. 2: Some of the spherical harmonic components of the potential of an As atom in the ideal surface of GaAs(110) for incident energy 50 eV and *fuzzy* parameter $a = 0.1$ Å.

dependence of the scattering properties of nonspherical potentials. We show the squared scattering amplitude $|A(\mathbf{k}', \mathbf{k})|$ in dependence of the direction of the outgoing plane wave vector $\mathbf{k}'$ in a polar plot. The incident plane wave vector $\mathbf{k}$ is fixed and indicated with an arrow pointing to the origin. For comparison we first show in figures 3 and 4 two sights of the polar diagram for a spherical symmetric muffin-tin potential, which we calculated from the phase shifts given by Meyer, Duke and Paton [7].

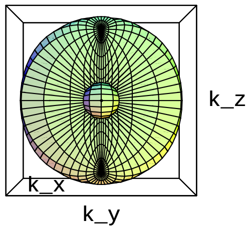

Fig. 3: Polar diagram of the squared scattering amplitude for a spherical symmetric muffin-tin potential of an As atom in GaAs at energy 50 eV. View along the incidence direction.

In consequence of the spherical symmetry of the potential the scattering amplitude shows cylindrical symmetry around the incident wave vector direction. The main electron flux goes into forward direction, a smaller portion is scattered almost perpendicular to the incident wave vector, and a small part is scattered backward.

In the next two figures 5 and 6 we plot the polar diagram for the As atom in the GaAs(110) bulk

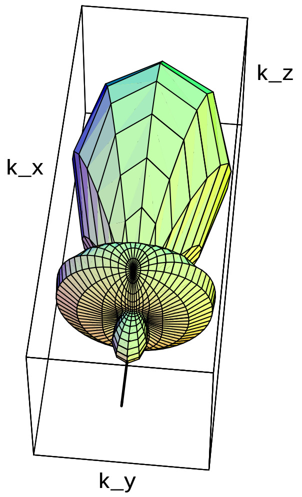

Fig. 4: Polar diagram of the squared scattering amplitude for a spherical symmetric muffin-tin potential of an As atom in GaAs at energy 50 eV. Top view.

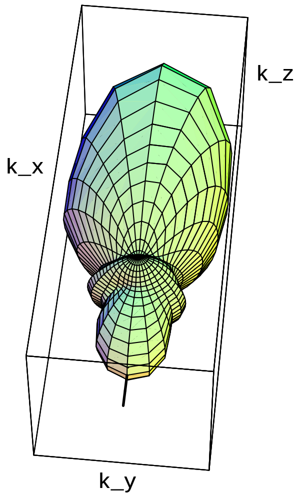

Fig. 6: Polar diagram of the squared scattering amplitude for the potential of an As atom in the bulk of GaAs(110) for perpendicular incidence at energy 50 eV. Top view.

geometry for an incident wavevector perpendicular to the surface at energy $E = 50$ eV.

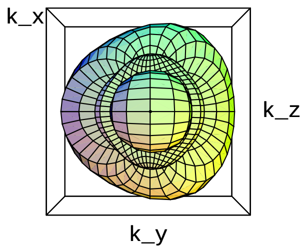

Fig. 5: Polar diagram of the squared scattering amplitude for the potential of an As atom in the bulk of GaAs(110) for perpendicular incidence at energy 50 eV. View normal to the crystal surface.

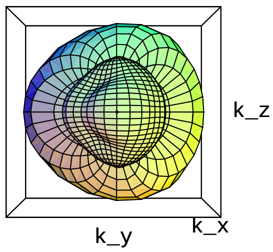

Fig. 7: Polar diagram of the squared scattering amplitude for the potential of an As atom in the ideal surface of GaAs(110) for perpendicular incidence at energy 50 eV. View normal to the crystal surface.

The mirror symmetry of the surface geometry is also recognizable by the scattering amplitude, and a considerable deviation from the cylindrical symmetry in the scattering amplitude of a spherical symmetric potential is to remark.

In another pair of figures 7 and 8 we show the squared scattering amplitude for the GaAs(110) surface geometry and normal incidence.

Here the deviations from the cylindrical symmetry are more distinct. The polar diagram bulges in the direction of the two gallium neighbors located on the right side of the arsenic scattering center in the same layer and towards the gallium atom at the left side in the second layer.

Furthermore we show in figures 9 and 10 the same situation as in figures 5 and 6, but for incidence energy $E = 20$ eV. In this case the backward scattering is comparable to that in forward direction.

In the last two figures 11 and 12 we plot the squared scattering amplitude again for an As atom in the GaAs(110) bulk geometry at electron energy 50 eV but for a non-normal incident wave vector $\mathbf{k}$.

The electron impinges along the mirror plane of the (110) surface under an angle of $\approx 26°$. These

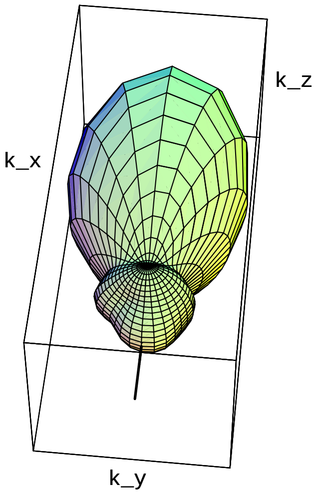

Fig. 8: Polar diagram of the squared scattering amplitude for the potential of an As atom in the ideal surface of GaAs(110) for perpendicular incidence at energy 50 eV. Top view.

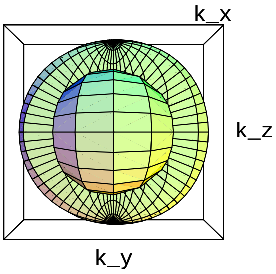

Fig. 9: Polar diagram of the squared scattering amplitude for the potential of an As atom in the bulk of GaAs(110) for perpendicular incidence at energy 20 eV. View normal to the crystal surface.

plots show that the form of the polar diagram for a non-spherical symmetric potential strongly depends on the incidence direction, whereas in the spherical symmetric case the polar diagram does not change its form, but only turns together with the incidence direction. This is important in multiple scattering because inside the crystal the scattering electrons impinge from all directions onto the crystal atoms.

REFERENCES

[1] W. H. Butler, A. Gonis, and X.-G. Zhang, Phys. Rev. B **45**, 11527 (1992).

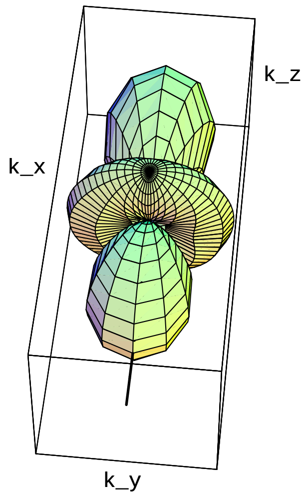

Fig. 10: Polar diagram of the squared scattering amplitude for the potential of an As atom in the bulk of GaAs(110) for perpendicular incidence at energy 20 eV. Top view.

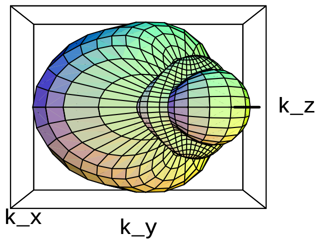

Fig. 11: Polar diagram of the squared scattering amplitude for the potential of an As atom in the bulk of GaAs(110) for non-normal incidence at energy 50 eV. View normal to the crystal surface.

[2] M. Grass, J. Braun, and G. Borstel, Phys. Rev. B **47**, 15487 (1993); J. Braun and G. Borstel, submitted to Phys. Rev. B.

[3] J. W. Krewer, W. Dürr, D. Pescia, and R. Feder, Sol. State Commun. **74**, 137 (1990); J. W. Krewer, and R. Feder, Physica B **172**, 135 (1991).

[4] S. Nagano and S. Y. Tong, Phys. Rev. B **32**, 6562 (1985).

[5] L. F. Shampine and M. K. Gordon, *Computer-Lösung gewöhnlicher Differentialgleichungen* (Vieweg, Braunschweig, 1984).

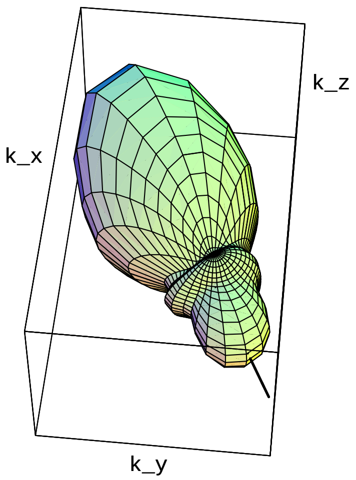

Fig. 12: Polar diagram of the squared scattering amplitude for the potential of an As atom in the bulk of GaAs(110) for non-normal incidence at energy 50 eV. Top view.

[6] E. Clementi and C. Roetti, Atomic Data Nucl. Data Tables **14**, 177 (1974).

[7] R. J. Meyer, C. B. Duke, and A. Paton, Surf. Sci. **97**, 512 (1980); W. K. Ford, C. B. Duke, and A. Paton, Surf. Sci. **115**, 195 (1982).

[8] V. I. Lebedev, U.S.S.R. Comput. Math. and Math. Phys. **16**, 10 (1976); Siberian Math. J. **18**, 99 (1977). We recalculated Lebedev's weight and point sets with Wolfram's *Mathematica* in the required accuracy.

[9] A. D. Becke, J. Chem. Phys. **88**, 2547 (1988).

[10] N. Stefanou and R. Zeller, J. Phys.: Condens. Matter **3**, 7599 (1991).